UPFLOW ALONG A BASEMENT FAULT REVEALED BY GEOTHERMAL NUMERICAL PRESSURE TRANSIENT ANALYSIS

Katie McLean[1,2]*, Julian McDowell[1], Fabian Sepulveda[1], Jun Seastres[1], Sadiq J. Zarrouk[2] and Samantha Alcaraz[3]

[1] Contact Energy Ltd., Wairakei Power Station, Taupo, New Zealand

[2] Department of Engineering Science, University of Auckland, Private Bag 90210, Auckland, New Zealand

[3] GNS Science, Wairakei Research Centre, Taupo, New Zealand

* katie.mclean@contactenergy.co.nz

Keywords: *Pressure transient analysis, numerical framework, well testing, linear flow regime, channel boundary, Ohaaki, conceptual model.*

ABSTRACT

The well BR49 was drilled in 1995 into the basement of the East Bank of Ohaaki Geothermal field, New Zealand. Recent pressure transient datasets measured in 2015 reveal a distinctive linear flow response. This is strong evidence that fluid flow in BR49 is controlled by flow along a fault plane in the otherwise-impermeable greywacke basement, which is highly significant for the conceptual model of this field.

It has not always been clear whether there are one or two upflows at Ohaaki. The main upflow under the West Bank is certain, however the presence of a secondary upflow under the East Bank has been a subject of ongoing debate. In the most recent conceptual model the greywacke basement has low permeability. A major liquid upflow is located in the northwest part of the field, which flows up through the West Bank and laterally to the East Bank; and a secondary upflow is located in the southeast underneath the East Bank. In spite of the implication for fault-related permeability in the greywacke, direct evidence for faults have been elusive. This study presents cumulative reservoir engineering, numerical modelling and geochemistry evidence, all of which supports the conclusion that BR49 must, in fact, be connected to a deep fault-controlled fluid source.

This study focuses on pressure transient analysis (PTA) results from well BR49 which provide direct evidence for a permeable fault in the basement. This powerfully demonstrates the value of performing PTA early, during completion testing, so the results can be used as inputs to the conceptual model. It is also a demonstration of the numerical PTA framework.

1. INTRODUCTION

BR49 was drilled in 1995 in the East Bank of Ohaaki Geothermal field, New Zealand. It has been a good production well supplying high-pressure steam to the power station. In 2015 it was selected for a trial of deflagration stimulation, and two injection/falloff tests were performed as part of that program. One outcome of these injection/falloff tests was the capture of high-quality pressure transient datasets. At the time of the deflagration trial the pressure transients were not analysed as the falloffs appeared to be badly affected by pressure rebound in late-time. Subsequently it became apparent that the early-time data reveals a characteristic flow regime not often seen in geothermal PTA data, which has important implications for the conceptual model of the field.

As the Ohaaki geothermal field has an existing conceptual model, this prompted some research into whether the PTA findings were consistent with this conceptual model. Many forms of data are used to build a conceptual model, including pressure and temperature data, geology, geophysics and geochemistry. All of these data sources relevant to the BR49 area are considered, to see if they are supportive of the PTA conclusions.

2. BACKGROUND

2.1 Regional setting

The Ohaaki geothermal system is located at the eastern margin of the Taupo Volcanic Zone (TVZ) in the North Island of New Zealand (Figure 1). The two production areas are referred to as East Bank (south-east of Waikato River) and West Bank (north-west of Waikato River). The production well BR49 is deviated towards the east, across the southern end of the East Bank (Figure 1).

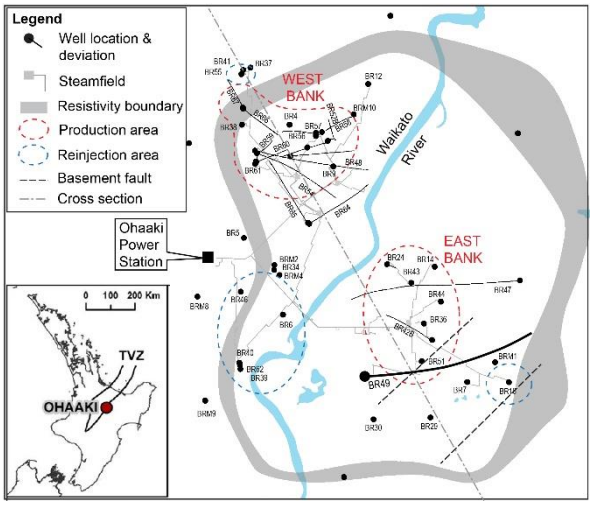

Figure 1: Map of Ohaaki geothermal system showing the West Bank and East Bank production areas, and also reinjection areas. BR49 is the deviated well in bold towards the south end of the East Bank area. The intersection of "East Fault" and "West Fault" (discussed in Section 5.1) with the top of the basement are shown with black dashed lines. NNW-SSE cross-section line (grey dashed line) is indicative of the location of all cross sections in this paper. Inset: regional map showing the location of Ohaaki.

2.2 Numerical pressure transient analysis

Pressure transient analysis (PTA) is a powerful tool capable of detecting reservoir features that control the flow of fluid near a well, such as stimulation or damage near the wellbore,

or reservoir boundaries. Historically, PTA has predominantly involved measuring the slope of straight lines on specialised plots of pressure transient datasets. Modern PTA utilises the pressure derivative plot (Bourdet, 2002) and uses software to match models to pressure transient datasets using non-linear regression techniques. The pressure derivative plot is a critical diagnostic tool, allowing selection of an appropriate model to fit the field data, as many flow regimes have characteristic pressure derivative shapes (Figure 2).

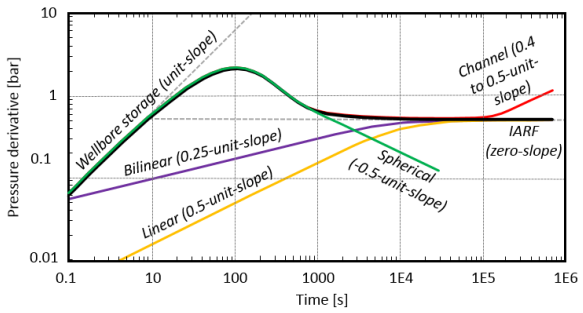

Figure 2: Derivative plot showing examples of characteristic response of various flow regimes, including: infinite-acting radial flow (IARF), linear flow, bilinear flow, spherical flow and a channel boundary (after Houzé et al., 2012).

The vast majority of modern PTA uses analytical models, which are relatively simple systems of linear equations used to calculate the model response. More complex systems such as geothermal reservoirs require the model response to be calculated numerically, which involves setting up a grid of blocks to represent the reservoir and using a numerical simulator to calculate the heat and mass flows between the blocks, and ultimately the pressure at the well block.

O'Sullivan et al. (2005) created numerical PTA software in which the model response was calculated using the simulator TOUGH2 (Pruess, 1999). Unfortunately this was developed for a private client and is not widely available. To enable numerical PTA, McLean and Zarrouk (2017a) developed a framework for the modelling, with guidelines on the grid setup and other simulation parameters. This was done using TOUGH2 automated by PyTOUGH (Croucher, 2011), but in principle can be used with any fluid flow simulator.

3. BR49 PRESSURE TRANSIENTS

3.1 Field data

The 1995 injection/falloff tests were three increasing flow steps, then a step down to the first flow rate. The transients were measured during the pressure falloff at the step down to the lower flow rate. A falloff to zero flow was deliberately avoided as zero flow means the well is heating during the transient, which can cause drift in the pressure measurement due to pressure pivoting, wireline stretch and downflows.

Both injection tests had the same design and the pressure transients measured were so similar that only one is shown here for simplicity, the one from the pre-deflagration test. The pressure transient is shown in a history plot in Figure 3 and the corresponding pressure derivative plot in Figure 4.

It was initially believed that the transient could not be modelled due to the rebound in the falloff (Figure 3). The rebound was attributed to pressure recovery in that region of the reservoir, due to the shut of multiple production wells during a flash plant outage.

It subsequently became apparent that the shape of the pressure transient has important implications for the conceptual model. The earlier part of the falloffs (first ~1 hour) reveal a characteristic linear flow regime. Also it was recognised that while pressure recovery does affect the data, a rebound in pressure during the falloff would be expected *regardless*, for this type of flow regime.

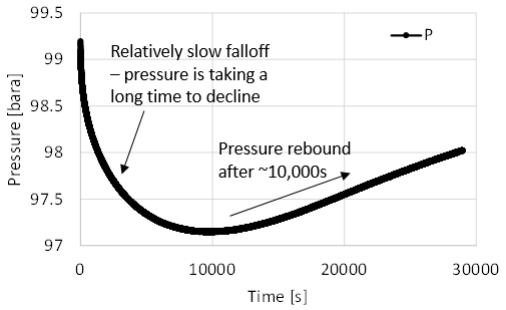

Figure 3: History plot of BR49 falloff pressure transient, showing rebound initially believed to be due only to pressure recovery in the area.

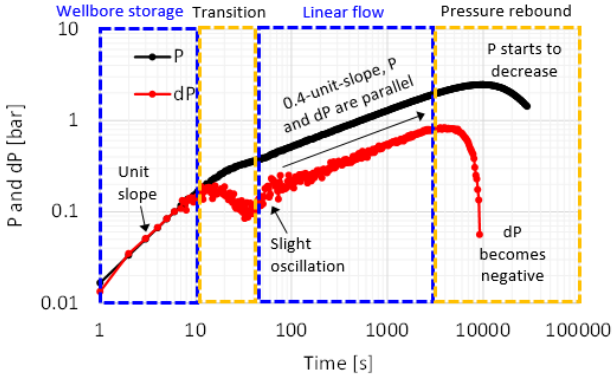

Figure 4: Derivative plot of BR49 falloff pressure transient, showing various stages: wellbore storage, transition, linear flow and apparent pressure rebound.

3.2 Narrow channel model

Scrutiny of the derivative plot of field data is useful to "diagnose" the test: to determine which model(s) is likely to fit the field data. The derivative plot for the BR49 transient (Figure 4) exhibits the following features:

1. First ~10s: short period of wellbore storage characterised by a unit-slope and both pressure (P) and derivative (dP) plotting along the same line.
2. 10 to 40s: the data transitions rapidly from (1) to (3), exhibiting a slight oscillation.
3. 40 to ~3000s: extended period where P and dP are divided but parallel, with a 0.4-unit-slope.
4. >3000s: pressure rebound dominates the test, causing dP to drop and become negative.

The parallel P and dP with 0.4-unit-slope (feature 3) are characteristic of a narrow channel model. Linear flow along a single near-well fracture was also considered, however this model type does not reproduce the wellbore storage or transition.

McLean and Zarrouk (2017b) developed a numerical channel model, with a central well block and radial grid blocks representing the reservoir. Reductions in the volumes and the surface areas of some of the blocks effectively represents two linear impermeable boundaries, shown schematically in Figure 5. Also seen in Figure 5 is that at first the flow regime is radial (before the boundaries are detected) and later the flow is linear along the channel. The narrower the channel the shorter the period of radial flow.

An example derivative plot of typical channel model results (Figure 6) shows that the pressure derivative (solid lines) has a characteristic 0.4-unit-slope (increasing slightly in late-time) and that the pressure data (dashed lines) show no particular behaviour. When the channel is very narrow (<10m for the model in Figure 6) the pressure and derivative lines become almost parallel. As the BR49 data exhibits these characteristics, this model was chosen to match the field data.

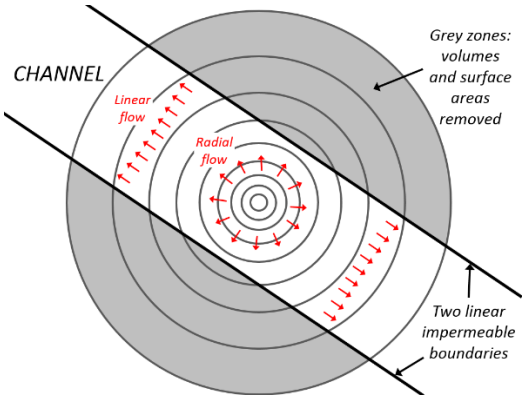

Figure 5: Schematic of channel model showing early radial flow followed by later linear flow along the channel.

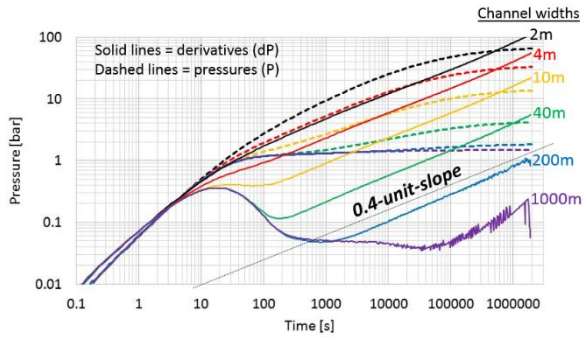

Figure 6: Example derivative plot of channel model simulated datasets, showing the effect of changing the channel widths (data from McLean and Zarrouk, 2017b).

Figure 7 shows the fit of the channel model to the BR49 field data. The variable parameters in the model were: reservoir permeability (k), well-to-boundary distance (L), skin factor (s), initial reservoir pressure (P_i), well compressibility (c).

The model match in Figure 7 was achieved by first manually adjusting the variable parameters to reasonable values, and then using the inversion software PEST (Doherty, 2010) to refine the parameters. The estimated values for the reservoir parameters were: k = 66 mD, s = 0.2, L = 2.5 m, P_i = 77 bara, c = 5.1×10^{-8} Pa^{-1}.

The model is a good match to the field data throughout the early-time wellbore storage period (unit-slope) and most of the intermediate-time linear flow period when the pressure and derivative are parallel (0.4-unit-slope). The transition between the wellbore storage period and the linear flow period is too slow in the model, though the exact shape of the field data is uncertain here due to the oscillation (Figure 7).

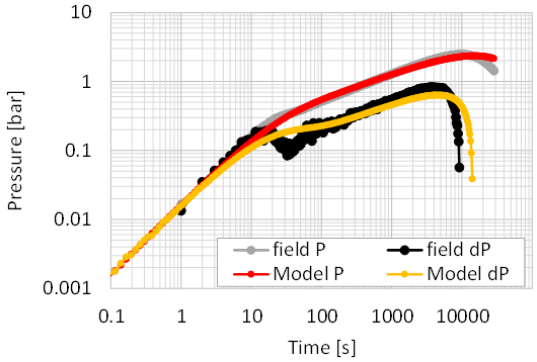

Figure 7: Derivative plot showing fit of channel model to BR49 field data.

The model results exhibit a rebound in the falloff, despite the fact that no pressure recovery of the surrounding area was included in the model. The modelled rebound is due to the superposition of the pressure buildups (due to injection step rate increases) with the pressure falloff. For this model type the pressure buildups do not level off and stabilise as they do for two-dimensional models of radial flow, but keep increasing, which has a significant effect on the subsequent falloff. This lack of stabilisation of the pressure buildups in the field data was noted during the assessment of the injectivity index.

The model match is not good in late time, however considering the fact that this model does not include any pressure recovery of the area (difficult to constrain), the overall match is surprisingly good (proof of concept). The model indicates that BR49 is dominated by linear flow along a feature approximately 5 m wide (double the well-to-boundary distance L). As this permeability is located in the greywacke basement this is strong evidence for the presence of a permeable fault there, as a fault is the only likely geological feature consistent with this result. This has important implications for the conceptual model of Ohaaki, where the presence of an upflow under the East Bank (requiring basement permeability) has been much debated.

4. CONCEPTUAL MODEL

This section presents the most recent conceptual model for Ohaaki (Mroczek et al., 2016). Some of the major reservoir-scale data that informs the conceptual model is presented here. More detailed investigations into the specific area around BR49 are presented in Section 5.

4.1 One upflow vs two upflows

The earliest debate regarding the upflows at Ohaaki was based on geochemical data. The first review of Ohaaki reservoir chemistry was by Mahon and Finlayson (1972) who interpreted a common source for West Bank and East Bank fluids based on substantial chemical similarities. There are differences such as the lower chloride concentration in the East Bank, which was attributed by Mahon and Finlayson (1972) to boiling and dilution processes. Others took a different view and in the same year that BR49 was drilled,

Giggenbach (1995) and Hulston and Lupton (1995) proposed that the differences in West Bank and East Bank chemistry result from two different sources of deep recharge (upflows). This was also the conclusion of a more recent study by Christenson et al. (2002).

Mroczek et al. (2016) build the case for the two-upflow model, taking into account all data sources including geochemistry, geology, geophysics and reservoir engineering data. The Mroczek et al. (2016) model proposes that:

1. A major liquid upflow rises up in the northwest part of the field (location offset with respect to the West Bank) flowing up through the West Bank and laterally to the East Bank.
2. A secondary upflow rises up through basement in the southeast underneath the East Bank.

The main features of the Mroczek et al. (2016) conceptual model can be seen in Figure 8.

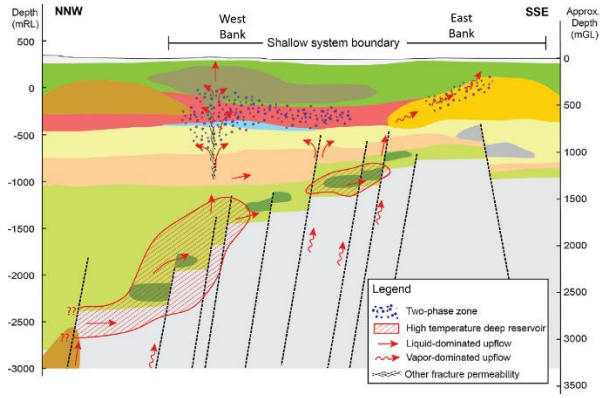

Figure 8: NNW-SSE cross section illustrating the conceptual model, including stratigraphy, faults and flow arrows. The two upflows can be seen, on the left (West Bank) and on the right (East Bank) (after Mroczek et al., 2016).

4.2 Geophysics

A key input to the conceptual model was a relatively recent 3D resistivity inversion model of MT data (Bertrand et al., 2015), shown in Figure 9. This resistivity inversion exhibits two deep low-resistivity anomalies in the basement. The top of the basement is located by gravity data and also by stratigraphy from drilled wells, both are shown in Figure 9.

The larger of the deep low-resistivity anomalies is interpreted as the primary upflow for Ohaaki, with fluid flowing laterally from this location through the volcanics on top of the basement, and the up into the West Bank. The smaller of the anomalies is interpreted as a secondary upflow (smaller than the primary upflow) which emerges into the East Bank.

Both upflows originate in the greywacke basement, and therefore require permeability there. Greywacke is generally impermeable and so permeability is expected to be secondary, associated only with faults/fracturing. Therefore it will be much more localised than in the volcanics above, and harder to intersect while drilling. This is supported by overall drilling/well testing experience at Ohaaki which shows that in general most wells have several feed zones throughout the volcanic sequence, and then none in the greywacke. The permeability is there in the basement, it is just harder to find.

5.5 Numerical model

Prior to 2017 the mass input into the base of the Ohaaki numerical model (run using TOUGH2) was applied broadly across the West and East banks with a weighting of overall mass on the former. With a broad mass input it was difficult to match individual well pressure recovery. A broad mass input was also seen to be at odds with the understanding that the basement was largely low permeability matrix with discrete faults providing the conduits for hot fluid upflow.

Following a detailed review of the model permeability and structure alongside the recent deep pressure recovery led to a simplification of the model structure and a redistribution of mass input to align with interpreted faults in the basement (Figure 10). The intention was to provide a model which captured the interpreted pathways for deep recharge, improved the pressure response and better aligned with the conceptual model.

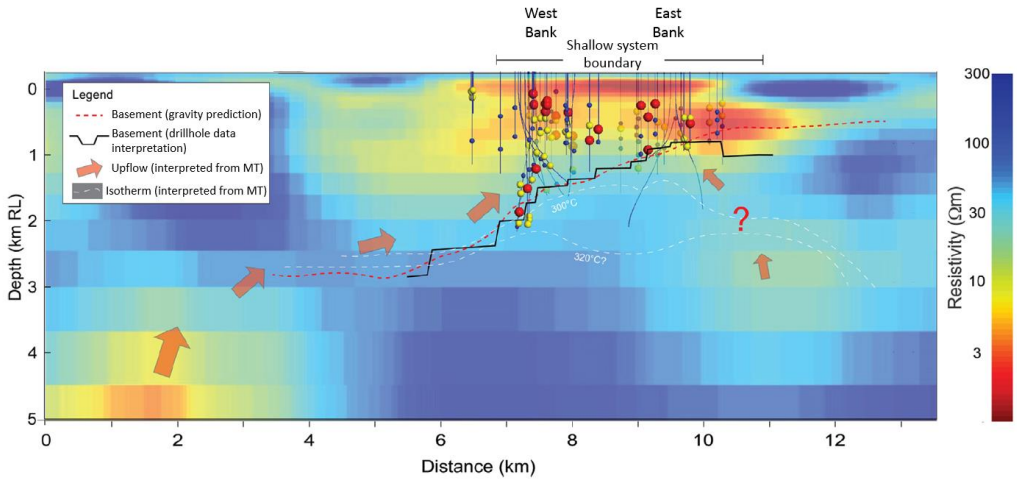

Figure 9: NNW-SSE cross section showing slice through 3D resistivity inversion model (after Mroczek et al., 2016).

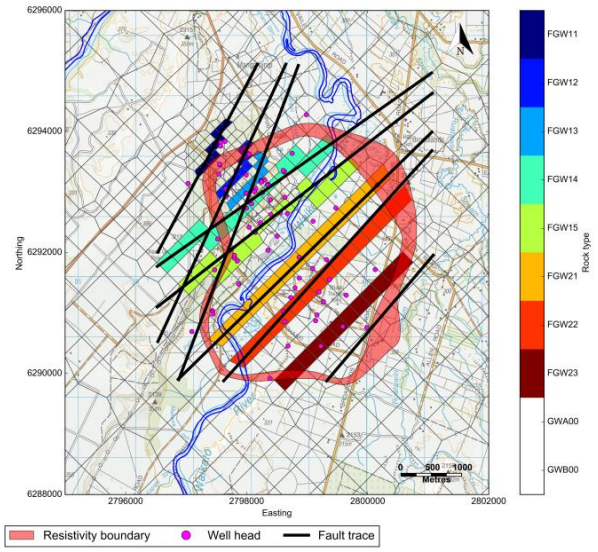

Figure 10: Postulated faults at Ohaaki with corresponding basement discrete mass input areas (Ratouis et al., 2017).

During the calibration process it was found that the implementation of the fault controlled mass input at the base of the model was the main reason for helping replicate the pressure recovery in deep wells which earlier model versions could not manage (Figure 11).

The current calibration efforts on the Ohaaki model include testing the benefit of incorporating more fracture representation in the shallow and intermediate parts of the reservoir to aid both pressure and enthalpy matching. Cooling of the intermediate reservoir at Ohaaki has been ongoing and considered to be linked to vertical conduits for shallow groundwater to migrate down into the reservoir (Ratouis *et al.*, 2017). Initial results have shown benefits to the matching using the approach of discrete fracture embedding. McDowell (2015) demonstrated the usefulness of this method in matching injection returns along an inferred structural pathway using a single porosity model.

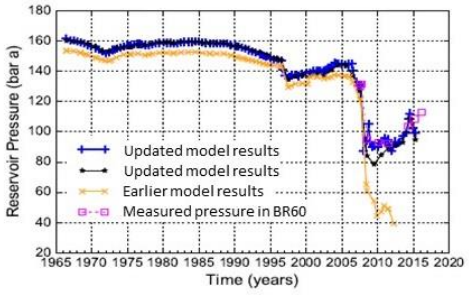

Figure 11: Pressure matching improvement following implementation of structurally linked mass upflows in the numerical model. Blue and black lines represent updated model, pink markers represent measured pressure (Ratouis et al., 2017).

The model does not yet explicitly represent the fault at BR49 through this study but now has a strong rationale for updating the conceptual understanding. To date the pressure and enthalpy of BR49 have not been well-matched by the numerical model, but with these new insights it should be possible to improve the calibration.

In general the PTA studies at BR49 help provide further support for the widespread implementation of discrete structurally controlled permeability in the basement at Ohaaki (as opposed to matrix only) and further demonstrates the power of sound investigative reservoir engineering to support numerical modelling.

5. DETAILED INVESTIGATION OF BR49 AND THE SURROUNDING AREA

The previous section considered reservoir-scale inputs to the conceptual model, which point to the two-upflow model and basement permeability in general. In this section the details of BR49 are presented, including geology, completion test data, pressure and temperature trends, and fluid chemistry trends. These are discussed in the context of the current conceptual model.

5.1 Geology of BR49

BR49 was drilled in 1995, deviated to target two NE-SW trending faults ("West Fault" and "East Fault") which were predicted to cut the greywacke basement on either side of a horst structure in the basement (Figure 12) (Wood and Rosenberg, 1995). These faults can also be seen in Figure 8 (to the right). A cross-section along the line of BR49 shows the geological model based on the stratigraphy intersected in BR49 and nearby wells (Figure 12).

The "West Fault" was confirmed by permeability at this location identified during the completion test. The extension of this fault with depth is unconfirmed. Wood and Rosenberg (1995) did not find evidence for massive fracturing and intense mineralization around this depth so they characterized the West fault as a "simple fault" (left fault, Figure 12).

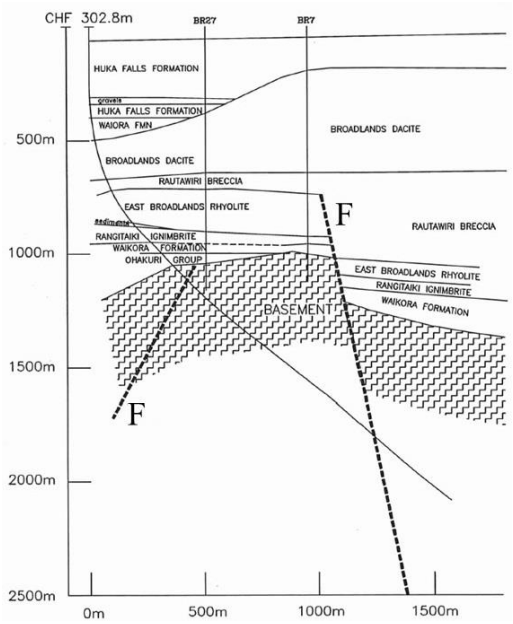

Figure 12: Geological cross section along BR49 (deviated well track) with nearby wells BR27 and BR7 (projected). Greywacke basement shown with shading. "West Fault" to the left and "East Fault" to the right (Wood and Rosenberg, 1995).

The location of the "East Fault" is still tentative as it is inferred only from stratigraphic offsets. It was not confirmed during the completion test, though this does not disprove the

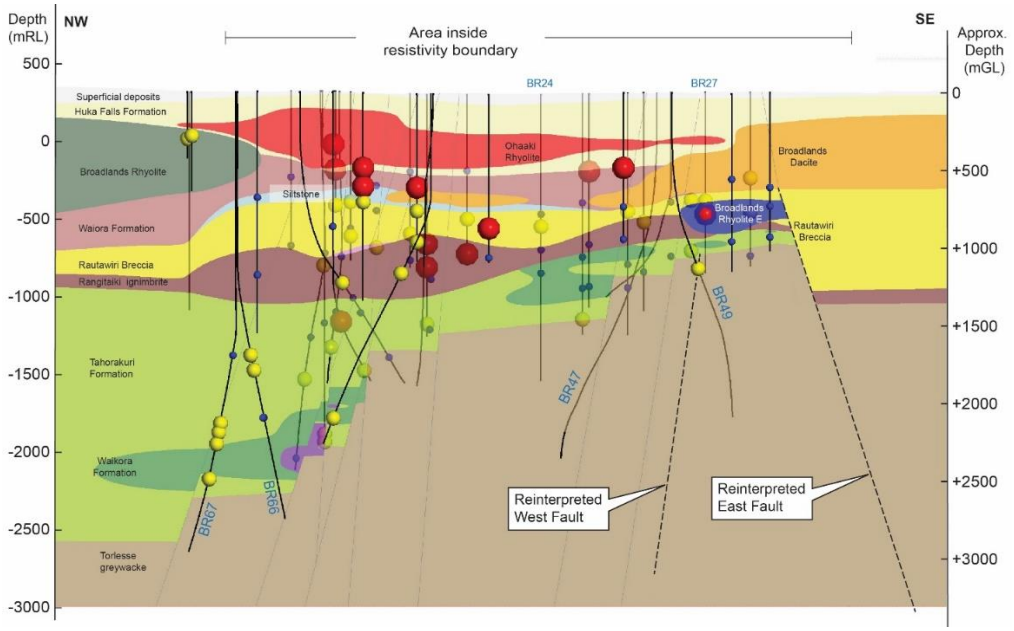

Figure 13: NW-SE striking geological cross section based on 3D geological model with re-interpretation of West and East Faults (nomenclature as in Wood and Rosenberg, 1995). Permeable zones from completion test data are classified as major (large red spheres), secondary (mid-sized yellow spheres) and minor (small blue spheres). Well labels shown for wells mentioned in text.

existence of the fault. This means either that the fault was not intersected by BR49, or that it is not permeable. A subdued low-resistivity anomaly under the East Bank (Figure 9) does align with the projection of the "East Fault". Also the prevailing geological model (Figure 13) indicates that BR49 did not intersect the "East Fault", in contrast to the earlier conclusion of Wood and Rosenberg (Figure 12).

The basement top in BR49 was well defined at 1160 mCHF by the intersection of greywacke (Wood and Rosenberg, 1995). The basement top in nearby BR27 was 69 m lower, an unlikely scenario, however the geology in BR27 was more uncertain as the cuttings from that depth were mixed and ambiguous. The mix of volcanics and argillite/greywacke could be interpreted either as Waikora formation (and therefore part of the volcanic sequence overlying the basement) or as greywacke contaminated with tuff (and hence part of the actual basement) (Wood and Rosenberg, 1995). The basement top in BR27 was later revised to be 76m higher, in line with BR49 (Rosenberg and Kilgour, 2006).

Permeability in BR49 was found at a depth of 1260 mCHF, 100m into the greywacke basement clearly identified at 1160 mCHF (Wood and Rosenberg, 1995). Although the basement top was considered to be clearly identified in BR49, due to the BR27 discussion there has been a perception that the basement top is ambiguous in BR49 also. For 20 years (until the 2015 testing) there has been confusion over whether the permeability at 1260m was really in the basement, or in the volcanics immediately above the basement.

5.2 Feed zone locations

The original completion test was carried out prior to discharge, likely with mud and cuttings partially blocking the feed zones (Bixley and Husted, 1995). Also the well is highly deviated (>50°) which means the spinner data is unreliable as the tool drags along the downside of the liner and cannot measure the established flow in the centre of the liner. Despite these limitations, the results of the 1995 completion test are consistent with results of the 2015 injection test.

The original 1995 completion test identified one major and one minor feed zone, both within the greywacke basement (Bixley and Husted, 1998):

- The major feed zone is at 1260 mCHF, interpreted from an increase in temperature gradient at this depth. This is confirmed by a discharging PTS (2 t/h bleed) which clearly shows a spike in temperature at this depth.
- The minor feed zone around 1500 mCHF is less certain, identified from spinner data.

The recent 2015 injection test at BR49 confirmed the major feed zone at 1260 mCHF, and also the presence of a feed zone below 1500 mCHF. The tool could not pass 1500 mCHF during the 2015 testing and so the second feed zone could not be located more accurately. This partial blockage is likely due to a buildup of cuttings or collapsed formation on the downside of the deviated liner.

5.3 Old pressure transient data

One pressure transient dataset measured during the original completion testing was considered useable, a falloff to zero flow. An MDH semilog plot analysis gives a very low transmissivity (*kh*) of 0.8 md (Grant, 1995). Interestingly, a log-log plot of the falloff (Figure 14) indicates a linear flow response (though it only persisted for around 2 minutes) interpreted as a fracture near the wellbore (Grant, 1995).

This dataset is not directly comparable to the pressure transients in this paper as it is a falloff to zero flow (to be avoided, as explained in Section 3.1) and the linear flow response appears to be much shorter. However, this type of response is rare in geothermal wells and indicated that flow to BR49 was different to usual.

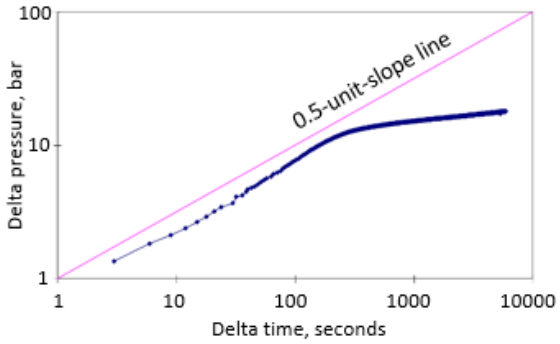

Figure 14: Log-log plot of falloff dataset from BR49 1995 completion test, showing 0.5-unit-slope response in early-time indicating a fracture response (after Grant, 1995).

5.4 BR49 vs West Bank reservoir pressure

The pressure in BR49 has been significantly higher than the wells in the West Bank, at all stages of the field development (Figure 15). This has been true for other East Bank wells, and quite early on was recognised as an indication of a separate upflow into the East Bank (Grindley, 1970). At the time of drilling, BR49 was also around 15 bar higher than other East Bank wells (Bixley and Husted, 1998).

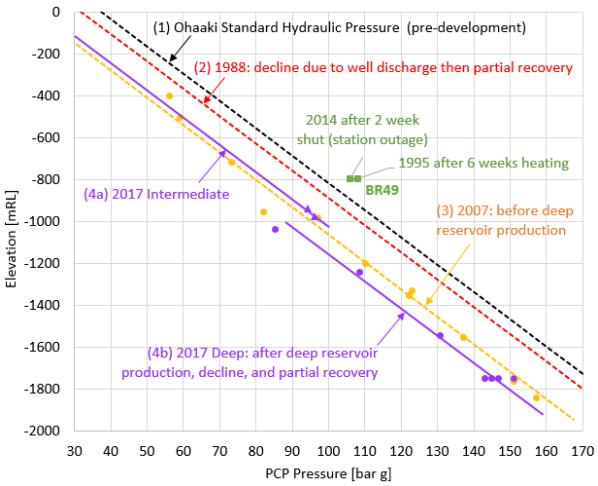

Figure 15: Pressure-for-depth plot of Ohaaki showing changes in the West Bank pressure profile at various stages from predevelopment (1) through to 2017 (4). BR49 on the East Bank is shown in green.

5.4 Reservoir chemistry

The East Bank wells are usually affected by inflow of cooler bicarbonate fluids which caused thermal deterioration, and eventually calcite deposition resulting from the inflow of these fluids. None of this chemical response occurred in BR49 and its mass flow remained generally within 130 t/h since deflagration in August 2015.

A plot of Cl/Ca and silica (quartz) temperature further characterised the uniqueness of BR49 chemistry (Figure 16). Typically in Ohaaki, as calcite deposition occurs, the Cl/Ca ratio increases with loss of calcium due to calcite precipitation at lower temperature and as such, the Ohaaki wells cluster along similar chemical trend. BR49 has a distinct trend as its fluid temperature (≥290°C) remained high and even its gas concentration is high at >1290 mmoles/100 moles (CO_2 total discharge) compared to <500 mmoles/100 moles in most East Bank wells.

Based on decreasing discharge enthalpy and increasing chloride total discharge, BR49 is primarily affected by boiling rather than inflow of cooler bicarbonate fluids. At this stage, there is no indication of mixing with cooler bicarbonate fluids in BR49. This well appears to be poorly connected to the western sector of the East Bank. The permeability of BR49 is likely controlled by vertical structure (basement fault) rather than a radial flow connection to other East Bank wells.

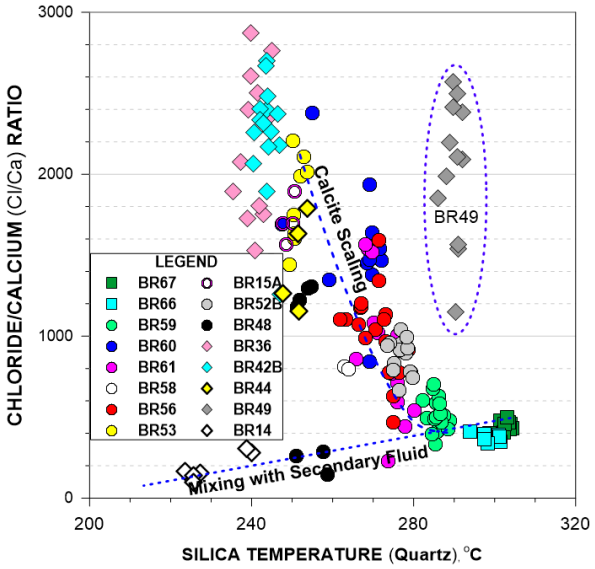

Figure 16: Cross-plot of chloride/calcium ratio and silica (quartz) temperature of Ohaaki production wells (2015-2017 chemistry data).

6. CONCLUSIONS

The BR49 pressure transient shows a linear flow response, which is a good match to a narrow channel model of approximately 5m width.

This is strong evidence for a permeable fault in the basement under the East Bank, independently confirming this hypothesis which previously relied on stratigraphic offsets and completion test data.

Fault permeability in the basement under the East Bank is key to the current conceptual model, which has a separate upflow under the East Bank. Geology, geochemistry, geophysics, reservoir engineering and numerical modelling all support this model.

As the pressure transient analysis (PTA) only occurred this year (2018) it simply supports the existing conceptual model (2016). The power of PTA comes from the fact that it is available much earlier than the other data, almost immediately after drilling. This is a powerful case for prioritizing PTA during completion testing, to make relevant

results such as those from BR49 available for inclusion in the conceptual model as early as possible.

ACKNOWLEDGEMENTS

The authors would like to thank Contact Energy Ltd. for the ongoing support and kind permission to publish this study.

REFERENCES

Bertrand, E.A., Caldwell, T.G., Bannister, S., Soengkono, S., Bennie, S.L., Hill, G.J. and Heise, W. (2016): *Using array MT data to image the crustal resistivity structure of the southeastern Taupo Volcanic Zone, New Zealand*, Journal of Volcanology and Geothermal Research, 305, 63-75.

Bixley, P.B. and Husted, M. (1998): *Ohaaki Completion Report BR49*. Contact Energy internal report, September 1998.

Bourdet, D. (2002): *Well Test Analysis: The Use of Advanced Interpretation Models*, Cubitt, J. ed., vol. 3, Elsevier.

Christenson, B.W., Mroczek, E.K, Kennedy, B.M., van Soest, M.C, Stewart, M.K. and Lyon, G. (2002): *Ohaaki reservoir chemistry: characteristics of an arc-type hydrothermal system in the Taupo Volcanic Zone, New Zealand*, Journal of Volcanology and Geothermal Research, 115(1), 53-82.

Croucher, A.E. (2011): *PyTOUGH: a Python Scripting Library for Automating TOUGH2 simulations*, Proceedings 33rd New Zealand Geothermal Workshop.

Doherty, J. (2010): *PEST: Model-Independent Parameter Estimation User Manual*, Watermark Numerical Computing.

Giggenbach, W.F. (1995): *Variations in the chemical and isotopic composition of fluids discharged from the Taupo Volcanic Zone, New Zealand*, Journal of Volcanology and Geothermal Research, 68, 89-116.

Grant, M.A. (1995): *Pressure transients in BR49*, MAGAK confidential client report, 20 July 1995.

Grindley, G.W. (1970): *Subsurface structures and relation to steam production in the Broadlands geothermal field, New Zealand*, Geothermics, special issue, 2, 248-261.

Houzé, O., Viturat, D. and Fjaere, O. (2012): *Dynamic Data Analysis: The Theory and Practice of Pressure Transient, Production Analysis, Well Performance Analysis, Production Logging and the use of Permanent Downhole Gauge Data*, KAPPA Engineering, v 4.12.03.

Hulston, J.R and Lupton, J.E. (1996): *Helium isotope studies of geothermal fields in Taupo Volcanic Zone, New Zealand*, Journal of Volcanology and Geothermal Research, 74(3-4), 297-321.

McDowell, J.M. (2015): *Discrete fracture embedding to match injection returns in a single porosity model.* Proceedings of World Geothermal Congress 2015.

McLean, K. and Zarrouk, S.J. (2016): *Application of numerical methods for geothermal pressure transient analysis: a deflagration case study from New Zealand*, Proceedings of Stanford Geothermal Workshop, California, USA.

McLean, K. and Zarrouk, S.J. (2017a): *Pressure transient analysis of geothermal wells: a framework for numerical modelling*, Renewable Energy 101, 737-746.

McLean, K. & Zarrouk, S. J. (2017b): *Geothermal Reservoir Channel Located by Pressure Transient Analysis: A Numerical Simulation Case Study*, in 'Geothermal Resources Council Transactions'.

Mroczek, E. K., Milicich, S. D., Bixley, P. F., Sepulveda, F., Bertrand, E. A., Soengkono, S. and Rae, A. (2016): *Ohaaki geothermal system: Refinement of a conceptual reservoir model*. Geothermics, 59, 311-324.

O'Sullivan, M. J., Croucher, A. E., Anderson, E. B., Kikuchi, T. and Nakagome, O. (2005): *An automated well-test analysis system (AWTAS)*, Geothermics 34(1), 3--25.

Pruess, K., Oldenburg, C. and Moridis, G. (1999): *TOUGH2 User's guide version 2.0*, Report LBNL-43134, Earth Sciences Division, Lawrence Berkeley National Laboratory., Berkeley (CA 94720, USA): University of California.

Ratouis, T.R., O'Sullivan, M.J., O'Sullivan, J.P., McDowell, J.M., Mannington, W.I. (2017). Holistic approaches and recent advances in the modelling of the Ohaaki geothermal system. Proceeding of New Zealand Geothermal Workshop 2017.

Rosenberg, M.D. and Kilgour, G.N. (2006): *Geology of Production Well BR51, Ohaaki Geothermal Field*, GNS Science Consultancy Report CR2006/08, January 2006.

Wood, C.P. and Rosenberg, M.D. (1995): *Geology of BR49, Ohaaki Geothermal Field*. Geological and Nuclear Sciences Ltd. Client Report 72537C.13C, October 1995.